A generalized Biot–Gassmann model for the acoustic properties of shaley sandstones[1]

José M. Carcione,[2,3] Boris Gurevich[4] and Fabio Cavallini[2]

Abstract

We obtain the wave velocities of clay-bearing sandstones as a function of clay content, porosity and frequency. Unlike previous theories, based simply on slowness and/or moduli averaging or two-phase models, we use a Biot-type three-phase theory that considers the existence of two solids (sand grains and clay particles) and a fluid. The theory, which is consistent with the critical porosity concept, uses three free parameters that determine the dependence of the dry-rock moduli of the sand and clay matrices as a function of porosity and clay content.

Testing of the model with laboratory data shows good agreement between predictions and measurements. In addition to a rock physics model that can be useful for petrophysical interpretation of wave velocities obtained from well logs and surface seismic data, the model provides the differential equation for computing synthetic seismograms in inhomogeneous media, from the seismic to the ultrasonic frequency bands.

Introduction

Successful interpretation of sonic logs and seismic data depends on a knowledge of the behaviour of wave propagation through rocks and geological units. In particular, sandstone reservoirs account for nearly 60% of oil reserves. In general, sandstones contain clay that considerably affects the seismic properties, such as compressional- and shear-wave velocities (Han, Nur and Morgan 1986). Previous attempts to model the effect of clay intrusions in sandstone assume empirical relationships (Tosaya and Nur 1982; Han *et al.* 1986) or a combination of empirical relationships and microstructural theories (Xu and White 1995; Goldberg and Gurevich 1998). While these models give reasonably good estimates of velocities from porosity and clay content, they are not always suitable for the calculation of synthetic seismograms, because they do not take dynamics into account.

Modelling the acoustic properties of shaley sandstones, that is, quantifying the variations of wave amplitudes and V_P and V_S versus porosity, clay content and
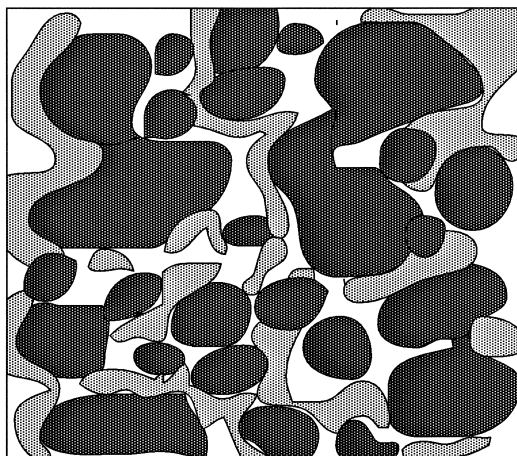
Figure 1. Interpenetrating sand (dark grey) and clay (light grey) matrices forming the composite skeleton of the shaley sandstone.

frequency, is achieved in the framework of Biot's theory of poroelasticity. This approach also provides the time-domain differential equations for calculation of synthetic seismograms in heterogeneous media.

For clay/sand mixtures, such an approach requires the consideration of a medium consisting of three phases: sand, clay and fluid. A three-phase Biot-type theory was recently developed by Leclaire, Cohen-Ténoudji and Aguirre-Puente (1994) for frozen porous media. This three-phase theory assumes that there is no direct contact between sand grains and ice, implying the existence of a water layer around the grains, isolating them from the ice. The model, which predicts three compressional waves and two shear waves, has recently been applied, with some minor modifications, to modelling the acoustic properties of permafrost (Carcione and Seriani 1998).

In this study, we replace ice by clay and include the terms responsible for the interaction between the sand grains (pure quartz grains) and the clay particles in the potential and kinetic energies. Lagrange's equations provide the differential equations of motion, and a plane-wave analysis gives the wave velocities and attenuation factors of the different modes. The bulk and shear moduli of the sand and clay matrices versus porosity are obtained from a relationship proposed by Krief *et al.* (1990). This relationship introduces two empirical parameters that can be obtained by calibrating the model with real data. An additional parameter provides one more degree of freedom for adjusting the velocity–porosity curves (at constant clay content) to the data.

The present model is somewhat similar to that recently proposed by Goldberg and Gurevich (1998). An important difference, however, is associated with our three-phase approach. Indeed, Goldberg and Gurevich (1998) assumed that the medium is composed of two phases: solid and fluid. The solid matrix, in turn, is a composite material, made of sand grains and clay particles. The elastic moduli of the solid/fluid

mixture were derived using the Gassmann equation. However, the latter is valid only when the solid matrix is homogeneous (Brown and Korringa 1975). This implies that the sand and clay particles are mixed homogeneously, forming, in effect, composite grains, which in turn form the rock matrix. Our three-phase approach is free of such assumptions, but it also implies a particular topological configuration, namely the one where sand and clay form two continuous and interpenetrating solid matrices (see Fig. 1). As an example, we test the model on the published data set of Han *et al.* (1986) and Klimentos and McCann (1990).

Model for clay-bearing sediments

The theory developed by Leclaire *et al.* (1994) explicitly takes into account the presence of three phases: solid substrate, ice and water. Here, we replace the ice with clay and include the contributions to the potential and kinetic energies due to the contact between the sand grains and the clay. In analogy with their notation, $\nu = 1, 2, 3$ denote sand, water and clay, respectively.

Following Leclaire *et al.* (1994), the equation of motion can be written in matrix form as

$$\mathbf{R}\,\mathrm{grad}\,\mathrm{div}\,\mathbf{u} - \boldsymbol{\mu}\,\mathrm{curl}\,\mathrm{curl}\,\mathbf{u} = \boldsymbol{\rho}\ddot{\mathbf{u}} + \mathbf{A}\dot{\mathbf{u}},$$

where $\mathbf{u}$ is the displacement field,

$$\mathbf{R} = \begin{pmatrix} R_{11} & R_{12} & R_{13} \\ R_{12} & R_{22} & R_{23} \\ R_{13} & R_{23} & R_{33} \end{pmatrix} \quad \text{and} \quad \boldsymbol{\mu} = \begin{pmatrix} \mu_{11} & 0 & \mu_{13} \\ 0 & 0 & 0 \\ \mu_{13} & 0 & \mu_{33} \end{pmatrix}$$

are the bulk and shear stiffness matrices, respectively, while

$$\boldsymbol{\rho} = \begin{pmatrix} \rho_{11} & \rho_{12} & \rho_{13} \\ \rho_{12} & \rho_{22} & \rho_{23} \\ \rho_{13} & \rho_{23} & \rho_{33} \end{pmatrix}$$

is the mass density matrix, and

$$\mathbf{A} = \begin{pmatrix} b_{11} & -b_{11} & 0 \\ -b_{11} & b_{11} + b_{33} & -b_{33} \\ 0 & -b_{33} & b_{33} \end{pmatrix}$$

is the friction matrix, where the parameter b_{13}, describing the interaction between the sand and clay matrices, has been assumed equal to zero. The fact that there is a frictionless connection between the two constituents can be interpreted as the sand and clay frames being welded (or bonded). There is an interchange of kinetic energy (described by ρ_{13}) and potential energy (described by R_{13} and μ_{13}) at the contact points, but no dissipation.

A dot above a variable denotes time differentiation. All the parameters with the subscript (13) describe the interaction between the two solid components. The elements of these matrices are obtained with the use of Lagrange's equations (Leclaire *et al.* 1994).

Appendix A summarizes the meaning of the different parameters, and Appendix B describes the form of the potential and kinetic energies. The porosity dependence of the sand and clay matrices is consistent with the concept of critical porosity, since the moduli should vanish above a certain value of the porosity (usually from 0.4 to 0.5). This dependence is determined by the empirical coefficients A_s and A_c (see equation (1)). This relationship was suggested by Krief *et al.* (1990) and applied to sand/clay mixtures by Goldberg and Gurevich (1998). Moreover, in some rocks there is an abrupt change of rock matrix properties with the addition of a small amount of clay, attributed to softening of cements, clay swelling and surface effects, i.e. the wave velocities decrease significantly when the clay content increases from 0 to a few per cent (Goldberg and Gurevich 1998). In order to model this effect, we multiply the shear modulus of the sand matrix by a factor depending on the empirical coefficient a (see equation (2): this factor tends to 1 when $a \rightarrow \infty$). Then, the bulk and shear moduli of the sand and clay matrices are assumed to satisfy the equations

$$K_{\mathrm{sm}} = K_{\mathrm{s}}\phi_{\mathrm{s}}(1 - \phi)^{A_{\mathrm{s}}/(1-\phi)}, \qquad K_{\mathrm{cm}} = K_{\mathrm{c}}\phi_{\mathrm{c}}(1 - \phi)^{A_{\mathrm{c}}/(1-\phi)} \tag{1}$$

and

$$\mu_{\mathrm{sm}} = \exp\{ - [(1 - C)C]^a\}K_{\mathrm{sm}}\mu_{\mathrm{s}}/K_{\mathrm{s}}, \qquad \mu_{\mathrm{cm}} = K_{\mathrm{cm}}\mu_{\mathrm{c}}/K_{\mathrm{c}}, \tag{2}$$

respectively. Note that $\phi + \phi_{\mathrm{s}} + \phi_{\mathrm{c}} = 1$ and $C = \phi_{\mathrm{c}}/(\phi_{\mathrm{c}} + \phi_{\mathrm{s}})$, whence ϕ_{c} and ϕ_{s} can be expressed in terms of porosity ϕ and clay content C, which prove to be the only independent variables of the model. Krief *et al.* (1990) set the parameters A_{s} and A_{c} at 3 regardless of the lithology, and Goldberg and Gurevich (1998) obtained values between 2 and 4. On the other hand, since $C(1 - C) < 1$, the exponential in (2) takes values between 0.166 (for $a = 0$) and 1 (for $a = \infty$). We found that reasonable values of parameter a are in the range [0,1].

The expressions (B6) for the density components, given in Appendix B, include the interaction between sand grains and clay particles, assuming that the grains flow through the clay matrix (as described by the tortuosity a_{13}) and that the clay particles flow through the sand skeleton (as described by a_{31}). As is well known, the tortuosity is related to the difference between the microvelocity and macrovelocity fields. If they are similar (i.e. for relatively rigid materials such as solids), the tortuosities equal 1, and these contributions vanish. However, these terms do contribute to the kinetic energy when the sand and clay matrices are unconsolidated or relatively unconsolidated, for which the tortuosities are greater than 1. As in Biot theory, we neglect the solid contributions related to the interaction with the saturating fluid.

If the properties of the clay equal those of the sand grains, then $\mathbf{u}_3 = \mathbf{u}_1$, $\theta_3 = \theta_1$, $d_3 = d_1$, and we obtain Biot's potential and kinetic energies, with the corresponding coefficients (see Appendix A), depending only on $\phi_{\mathrm{s}} + \phi_{\mathrm{c}}$. Moreover, when $\phi \rightarrow 1$,

the compressional-wave velocity tends to the wave velocity in the fluid, and the shear-wave velocity vanishes.

The reference frequency f_c, which determines the validity of the theory, $f \ll f_c$, is given by

$$f_c = \frac{\phi \eta_f}{2\pi T \rho_f \kappa}, \tag{3}$$

where we assume that the permeability is $\kappa = \phi_s \kappa_s + \phi_c \kappa_c$ (see Appendix B) and that the tortuosity is obtained from $1/T \approx (1 - C)/a_{21} + C/a_{23}$.

The three compressional-wave velocities of the three-phase porous medium are given by

$$V_{Pm} = [\text{Re}(\sqrt{\Lambda_m})]^{-1}, \qquad m = 1, 2, 3, \tag{4}$$

where Re denotes the real part, and Λ_m are obtained from the generalized characteristic equation $\det[\Lambda \mathbf{R} - \tilde{\boldsymbol{\rho}}] = 0$, which yields

$$\Lambda^3 \det[\mathbf{R}] - \Lambda^2 \text{tr}[\bar{\mathbf{R}}\tilde{\boldsymbol{\rho}}] + \Lambda \text{tr}[\mathbf{R}\bar{\tilde{\boldsymbol{\rho}}}] - \det \tilde{\boldsymbol{\rho}} = 0,$$

where tr denotes the trace, the overbar denotes the cofactor matrix (e.g. Fedorov 1968), and the effective density matrix,

$$\tilde{\boldsymbol{\rho}} = \boldsymbol{\rho} - i\mathbf{A}/\omega,$$

is defined in the frequency domain.

Likewise, the two shear-wave velocities V_{Sm} are given by

$$V_{Sm} = [\text{Re}(\sqrt{\Omega_m})]^{-1}, \qquad m = 1, 2, \tag{5}$$

where Ω_m are the complex solutions of the equation

$$\Omega^2 a' - \Omega b' + \det(\tilde{\boldsymbol{\rho}}) = 0,$$

with $a' = \text{tr}[\bar{\boldsymbol{\mu}}\tilde{\boldsymbol{\rho}}]$ and $b' = \text{tr}[\boldsymbol{\mu}\bar{\tilde{\boldsymbol{\rho}}}]$.

Following Dutta and Ode (1983), the magnitudes of the attenuation vectors (in dB) are given by

$$\alpha_{Pm} = 17.372\pi \frac{\text{Im}(\sqrt{\Lambda_m})}{\text{Re}(\sqrt{\Lambda_m})}, \qquad m = 1, 2, 3, \tag{6}$$

and

$$\alpha_{Sm} = 17.372\pi \frac{\text{Im}(\sqrt{\Omega_m})}{\text{Re}(\sqrt{\Omega_m})}, \qquad m = 1, 2. \tag{7}$$

Examples

We calibrate the model with the data sets published by Han *et al.* (1986) and Klimentos and McCann (1990), obtained at a confining pressure of 40 MPa. Han

Table 1. Material properties of the clay-bearing sandstone.

Solid grain	Bulk modulus, K_s	39 GPa
	Shear modulus, μ_s	39 GPa
	Density, ρ_s	2650 kg/m^3
	Average radius, R_s	50 μm
Clay	Bulk modulus, K_c	20 GPa
	Shear modulus, μ_c	10 GPa
	Density, ρ_c	2650 kg/m^3
	Average radius, R_c	1 μm
Fluid	Bulk modulus, K_f	2.4 GPa
	Density, ρ_f	1000 kg/m^3
	Viscosity, η_f	1.798 cP
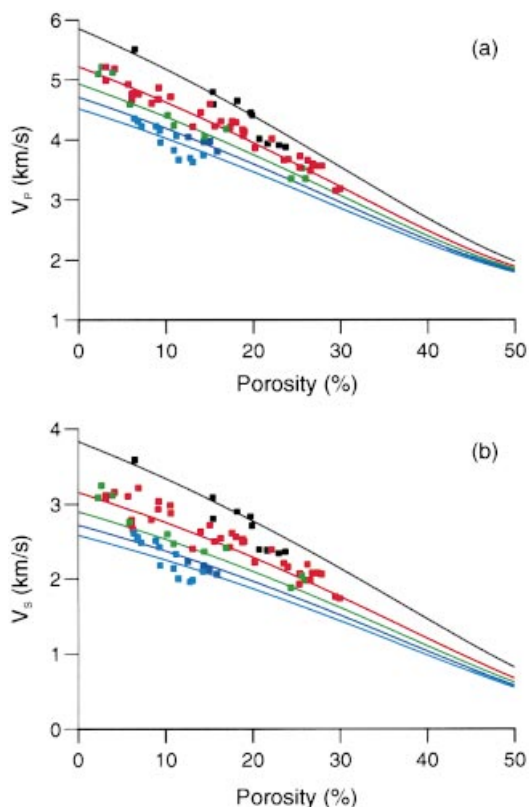
Figure 2. Velocities of compressional (a) and shear (b) fast waves versus porosity ϕ for different values of clay content C: black: $C = 0\%$; red: $C = 10\%$; green: $C = 20\%$; blue: $C = 30\%$, and light blue: $C = 40\%$. The experimental points correspond to the data published by Han *et al.* (1986). In this case, black, red, green, blue and light blue correspond to C values in the ranges $[C, C + 5\%]$, $C = 0, ..., 40\%$. The frequency is 5 kHz.
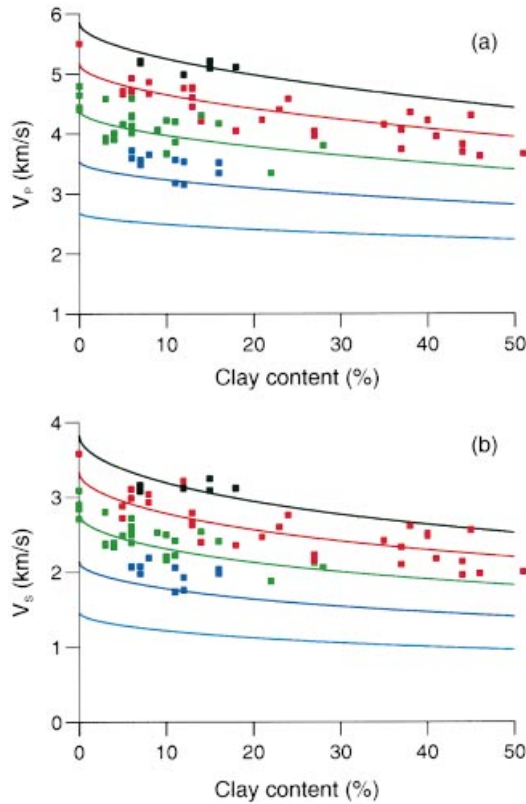
Figure 3. Velocities of compressional (a) and shear (b) fast waves versus clay content C for different values of porosity ϕ: black: $\phi = 0\%$; red: $\phi = 10\%$; green: $\phi = 20\%$; blue: $\phi = 30\%$, and light blue: $\phi = 40\%$. The experimental points correspond to the data published by Han *et al.* (1986). In this case, black, red, green, blue and light blue correspond to ϕ values in the ranges $[\phi, \phi + 5\%]$, $\phi = 0, \ldots, 40\%$. The frequency is 5 kHz.

et al. (1986) provide ultrasonic measurements of V_P and V_S for 75 sandstone samples with porosities ranging from 2 to 30% and a volume clay content from 0 to 50%. One feature of this data set is that a small amount of clay significantly softens the rock moduli, leading to reduced velocities. Table 1 shows the properties of the different constituents, and the prediction of the theory against the measurements obtained by Han *et al.* (1986) is shown in Figs 2a and b, where $A_s = A_c = 2$ and $a = 0.5$ (see equations (1) and (2)). The reference frequency (3) is $f_c = 84, 140, 18$ and 25 kHz for $(\phi, C) = (0.1, 0), (0.1, 0.4), (0.3, 0)$ and $(0.3, 0.4)$, respectively. Since the theory is valid below these reference frequencies, we assume a frequency of 5 KHz to fit the experimental data. Strictly speaking, this is not correct since the data have been acquired at ultrasonic frequencies of the order of hundreds of kHz. However, it is well known that Biot-type dissipation mechanisms alone do not account for the level of attenuation observed in rocks (Dvorkin, Nolen-Hoeksema and Nur 1994). A correct
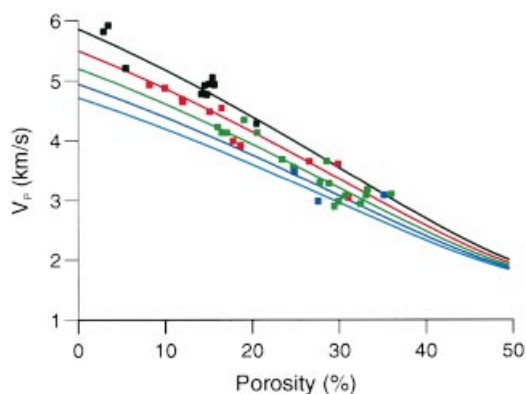
Figure 4. Compressional-wave velocity versus porosity for different values of clay content C: black: $C = 0\%$; red: $C = 10\%$; green: $C = 20\%$; blue: $C = 30\%$, and light blue: $C = 40\%$. The experimental points correspond to the data published by Klimentos and McCann (1990). In this case, black, red, green, blue and light blue correspond to C values in the ranges $[C, C + 5\%]$, $C = 0, ..., 40\%$. The frequency is 5 kHz.

description of this phenomenon would require the generalization of the different stiffness moduli to relaxation functions (Biot 1962). However, this fact reflects the robustness of the model for this particular example. Figure 2 shows the compressional- and shear-wave velocities versus porosity, where each curve corresponds to a different value of the clay content C. The root-mean-square deviation computed for all samples, apart from five outliers for P-waves and seven outliers for S-waves, is 93 m/s for the P-wave velocity and 100 m/s for the S-wave velocity. The match between theoretical and experimental data is quite good taking into account the fact that we used just two fitting parameters and did not use a rigorous parameter estimation algorithm. The values for A_s and A_c were chosen to obtain a reasonable fit of the data. The fact that $A_s = A_c$ is a satisfactory choice indicates the flexibility of the model in this case. In order to obtain a better agreement between theory and experiment, an inversion procedure, like that presented by Goldberg and Gurevich (1998), should be used. On the other hand, Fig. 3 represents the same velocities versus clay content C for porosities ranging from zero to 40%. The rapid decrease in wave velocity at low clay content is evident.

Figure 4 shows the compressional-wave velocity compared with the experimental points obtained by Klimentos and McCann (1990). In this case $a = 1$, since the softening of the rock moduli by clay is less pronounced than in the previous case. This data set was obtained at a confining pressure of 40 MPa, which, according to the authors, is equivalent to a depth of burial of about 1.5 km. For an average sediment density of 2300 kg/m³, this requires a pore pressure of 19 MPa, and therefore an overpressure of approximately 4.5 MPa. In fact, the porosities are higher than those expected at 1.5 km depth. Pore pressure, together with the confining pressure, determines the differential pressure which, in turn, determines the dry-rock bulk
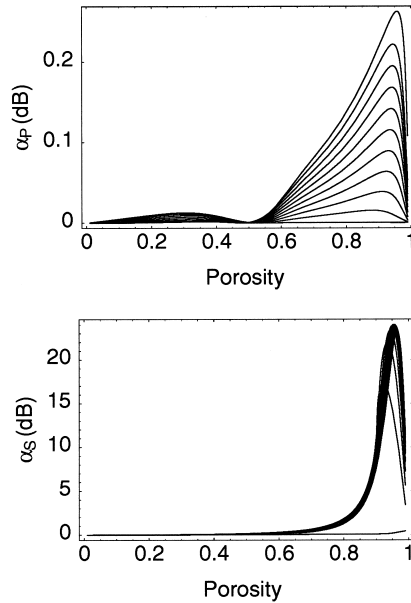
Figure 5. Compressional (a) and shear (b) attenuations in dB versus porosity for different values of clay content, which varies in steps of 0.1 from 0 to 1. The frequency is 25 Hz. Curves with higher peaks correspond to lower clay content.

moduli and porosity (Zimmerman, Somerton and King 1986). Hence, the pressure dependence is mainly contained in (1) and (2) through the porosity ϕ and the parameters A_s, A_c and a. Second-order effects can be due to the dependence on pressure and temperature of the fluid properties (Batzle and Wang 1992).

The attenuations (6) and (7) for the fast waves in the seismic band are shown in Fig. 5. In general, the higher the porosity the higher the dissipation. For completeness, Fig. 6 shows the phase velocities, computed using (4) and (5), and attenuations, computed using (6) and (7), of the slow compressional modes and the slow shear mode for a frequency of 25 Hz. Note that the attenuations of the slow modes are much higher than the attenuations of the fast modes, as expected. Modes have been numbered in order of decreasing phase speed.

It is important to note that the main advantage of the present model is not the accuracy of the prediction (empirical relationships may perform equally well), but the fact that it is a model based on physical grounds and is potentially useful for the inversion of rock properties and the computation of synthetic seismograms.

Conclusions

We have developed a new velocity-porosity-clay model that can be used for inversion applications such as sonic-log interpretation, lithological inversion of seismic data, AVO
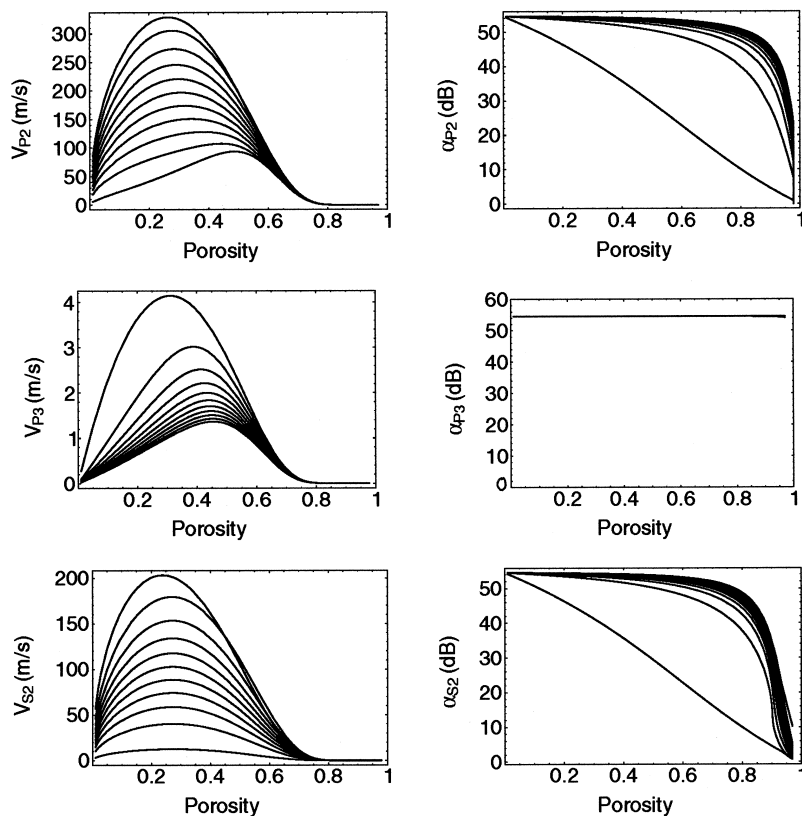
Figure 6. Phase velocities in m/s (left) and attenuations in dB (right) versus porosity ϕ for different values of clay content, which varies in steps of 0.1 from 0 to 1. The top and centre plots correspond to the slow compressional modes, and bottom plots to the slow shear mode. Higher curves correspond to higher clay content in the top left, bottom left and centre right frames; the opposite happens in the other cases.

inversion, etc. The model is based on a Biot-type formulation of the equation of motion, and therefore the number of free parameters is limited to a minimum. In principle, three parameters are used to obtain the bulk and shear moduli of the sand and clay matrices versus porosity and clay content. In the present study, two parameters were enough to fit the experimental data. Since the model is based on a Biot formulation, additional compressional and shear waves are predicted by the theory. For completeness, the characteristics (phase velocity and attenuation) of these modes are briefly outlined. Besides the inversion applications mentioned above, the formulation provides the differential equations for computing synthetic seismograms in inhomogeneous porous media.

Acknowledgements

Rock project, and by the European Union under the project 'Detection of overpressure zones with seismic and well data'. We thank the Associate Editor and Dr B. Trietsch for detailed reviews.

Appendix A

List of symbols

A   friction matrix;
A_s dimensionless empirical parameter; see equation (1);
A_c dimensionless empirical parameter; see equation (1);
a dimensionless empirical parameter; see equation (2);
a_{21} tortuosity for the fluid flowing through the sand matrix (see Appendix B.2);
a_{13} tortuosity for the sand grains flowing through the clay matrix (see Appendix B.2);
a_{23} tortuosity for fluid flowing through the clay matrix (see Appendix B.2);
a_{31} tortuosity for the clay flowing through the sand matrix (see Appendix B.2);
b_{11} friction coefficient between the sand grains and the fluid (see Appendix B.3);
b_{33} friction coefficient between the clay and the fluid (see Appendix B.3);
C clay content: $\phi_c/(\phi_c + \phi_s)$;
c_1 consolidation coefficient of the sand matrix: $K_{sm}/(\phi_s K_s)$;
c_3 consolidation coefficient of the clay matrix: $K_{cm}/(\phi_c K_c)$;
d_ν deviator $(\nu = 1, 3)$;
E_K kinetic energy;
E_P potential energy;
F viscous resistance force;
f_c reference frequency;
g_1 consolidation coefficient of the sand matrix: $\mu_{sm}/(\phi_s \mu_s)$;
g_3 consolidation coefficient of the clay matrix: $\mu_{cm}/(\phi_c \mu_c)$;
K_c bulk modulus of clay; see Table 1;
K_f fluid bulk modulus; see Table 1;
K_s bulk modulus of the sand grain; see Table 1;
K_{av} average bulk modulus: $[(1 - c_1)\phi_s/K_s + \phi/K_f + (1 - c_3)\phi_c/K_c]^{-1}$;
K_{cm} bulk modulus of the clay matrix; see equation (1);
K_{sm} bulk modulus of the sand matrix; see equation (1);
R   bulk stiffness matrix;
q   relative displacement vector;
r   relative displacement vector;
R average radii of sand and clay particles;
R_{11}: $K_1 + 4\mu_{11}/3 = [(1 - c_1)\phi_s]^2 K_{av} + K_{sm} + 4\mu_{11}/3$;
R_{12}: $C_{12} = (1 - c_1)\phi_s \phi K_{av}$;
R_{13}: $C_{13} = (1 - c_1)(1 - c_3)\phi_s \phi_c K_{av}$;
R_{22}: $\phi^2 K_{av}$;

R_{23}: $C_{23} = (1 - c_3)\phi_c \phi K_{av}$;

R_{33}: $K_3 + 4\mu_{33}/3 = [(1 - c_3)\phi_c]^2 K_{av} + K_{cm} + 4\mu_{33}/3$;

$\boldsymbol{\rho}$ mass density matrix;

$\tilde{\boldsymbol{\rho}}$ effective density matrix;

r_{12} geometrical aspect of the boundary separating the sand grains from the fluid phase;

r_{13} geometrical aspect of the boundary separating the sand grains from the clay;

r_{23} geometrical aspect of the boundary separating the clay from the fluid phase;

r_{31} geometrical aspect of the boundary separating the clay from the sand grains;

T average tortuosity;

V_{Pm} P-wave phase velocity ($m = 1, 2, 3$);

V_{Sm} S-wave phase velocity ($m = 1, 2$);

$\mathbf{s}$ microscopic particle-velocity vector;

$\mathbf{t}$ microscopic particle-velocity vector;

$\mathbf{u}_\nu$ displacement vector ($\nu = 1, 2, 3$);

$\mathbf{v}_\nu$ microscopic particle-velocity vector ($\nu = 1, 3$);

v average velocity of grains moving in the fluid;

$\mathbf{w}_\nu$ relative displacement vector ($\nu = 1, 3$);

$\boldsymbol{\alpha}_1$ fluid/sand matrix coefficient;

$\boldsymbol{\alpha}_3$ fluid/clay matrix coefficient;

$\boldsymbol{\beta}_1$ clay/sand matrix coefficient;

$\boldsymbol{\beta}_3$ sand/clay matrix coefficient;

α_{Pm} P-wave attenuation factor ($m = 1, 2, 3$);

α_{Sm} S-wave attenuation factor ($m = 1, 2$);

η_f fluid viscosity; see Table 1;

κ_s permeability of the sand matrix (see Appendix B.3);

κ_c permeability of the clay matrix (see Appendix B.3);

κ average permeability;

Λ_{Pm} P-wave root of the dispersion equation ($m = 1, 2, 3$);

μ_c shear modulus of the clay; see Table 1;

μ_s shear modulus of the sand grains; see Table 1;

μ_{cm} shear modulus of the clay matrix; see equation (2);

μ_{sm} shear modulus of the sand matrix; see equation (2);

$\boldsymbol{\mu}$ shear stiffness matrix;

μ_{11} same as μ_{sm};

μ_{13} shear coupling between the sand and clay matrices;

μ_{33} same as μ_{cm};

ν index denoting sand (1), water (2) and clay (3);

Ω_{Sm} S-wave root of the dispersion equation ($m = 1, 2$);

ω angular frequency: $2\pi f$;

ϕ_c proportion of clay;

ϕ proportion of fluid or porosity;

ϕ_s proportion of sand grains;

ρ_c clay density; see Table 1;
ρ_f fluid density; see Table 1;
ρ_s sand density; see Table 1;
$\rho_{\nu\nu'}$ generalized mass coefficients (see Appendix B.2);
θ_ν dilatation ($\nu = 1, 2, 3$).

Appendix B

Energies and friction coefficients

In their model of a frozen porous medium, Leclaire *et al.* (1994) assumed that there is no direct mechanical contact between the solid and ice, because they are separated by water. The model is generalized here in order to include the interaction between the sand grains and the clay, which corresponds to ice, and the coefficients of the dissipation potential. Following their notation, $\mathbf{u}_\nu$, for $\nu = 1, 2, 3$, denote the displacement vectors of sand, water and clay, respectively.

B1. Potential energy density

The total potential energy of the system can be expressed as

$$E_P = \mu_{11}d_1^2 + \frac{1}{2}K_1\theta_1^2 + C_{12}\theta_1\theta_2 + \frac{1}{2}K_2\theta_2^2 + C_{23}\theta_2\theta_3 + \frac{1}{2}K_3\theta_3^2 + \mu_{33}d_3^2$$
$$+ C_{13}\theta_1\theta_3,$$

where θ_ν and d_ν are the invariants of the strain tensor, called dilatations and deviators, while K_ν and $\mu_{\nu\nu'}$ are, respectively, the bulk and shear moduli of the effective phases.

All the parameters, except C_{13}, are as given by Leclaire *et al.* (1994), although sand/clay interactions are now taken into account. In order to calculate C_{13}, we generalize the elastic moduli obtained for the two-phase Biot's theory. For a medium with a proportion of sand ϕ_s and a porosity ϕ, the elastic moduli are

$$K_1 = (1 - c_1)^2\phi_s^2 K_a,$$

$$C_{12} = (1 - c_1)\phi_s\phi K_a, \tag{B1}$$

$$K_2 = \phi^2 K_a,$$

where

$$K_a = \left[(1 - c_1)\frac{\phi_s}{K_s} + \frac{\phi}{K_f}\right]^{-1}, \qquad c_1 = \frac{K_{sm}}{\phi_s K_s}.$$

Here K_s and K_f are the solid and fluid bulk moduli, K_a is the average bulk modulus, K_{sm} is the solid matrix bulk modulus, and c_1 is the bulk consolidation coefficient, such that $c_1 = 0$ for a suspension of solid grains in a fluid, and $c_1 = 1$ for a situation where

the grains form a monolithic block. Note that equations (B1) correspond to an effective solid porosity $\phi'_s = (1 - c_1)\phi_s$. If we replace the fluid by clay, the equations should read

$$K_1 = \phi'^2_s K_a,$$

$$C_{13} = \phi'_s \phi'_c K_a,$$

$$K_3 = \phi'^2_c K_a,$$

where

$$K_a = \left[\frac{\phi'_s}{K_s} + \frac{\phi'_c}{K_c} \right]^{-1}, \qquad \phi'_c = (1 - c_3)\phi_c, \qquad c_3 = \frac{K_{cm}}{\phi_c K_c}.$$

Here c_3 is the bulk consolidation coefficient of the clay matrix, with bulk modulus K_{cm}. For the three-phase system, the generalization of K_a to

$$K_{av} = \left[\frac{\phi'_s}{K_s} + \frac{\phi'_c}{K_c} + \frac{\phi}{K_f} \right]^{-1}$$

gives

$$K_1 = (1 - c_1)^2 \phi_s^2 K_{av},$$

$$C_{13} = (1 - c_1)\phi_s (1 - c_3)\phi_c K_{av},$$

$$K_3 = (1 - c_3)^2 \phi_c^2 K_{av},$$

$$K_{av} = \left[(1 - c_1)\frac{\phi_s}{K_s} + (1 - c_3)\frac{\phi_c}{K_c} + \frac{\phi}{K_f} \right]^{-1}.$$

B.2 Kinetic energy density

The kinetic energy is a function of the local velocities $\dot{\mathbf{u}}_1$, $\dot{\mathbf{u}}_2$ and $\dot{\mathbf{u}}_3$, where the dot denotes time differentiation. Generalizing Leclaire *et al.*'s (1994) kinetic energy, we get

$$E_K = \frac{1}{2}\rho_{11} \| \dot{\mathbf{u}}_1 \|^2 + \frac{1}{2}\rho_{22} \| \dot{\mathbf{u}}_2 \|^2 + \frac{1}{2}\rho_{33} \| \dot{\mathbf{u}}_3 \|^2$$
$$+ \rho_{12}\dot{\mathbf{u}}_1 \cdot \dot{\mathbf{u}}_2 + \rho_{23}\dot{\mathbf{u}}_2 \cdot \dot{\mathbf{u}}_3 + \rho_{13}\dot{\mathbf{u}}_1 \cdot \dot{\mathbf{u}}_3,$$

where, for simplicity, we omit the tilde above the density components.

We now want to determine the induced mass tensor ρ_{ij}. To this purpose we first deduce an expression for the kinetic energy through a microstructural argument and then compare the result with (B2). Let us define the macroscopic velocities

$$\dot{\mathbf{w}}_1 = \phi(\dot{\mathbf{u}}_2 - \dot{\mathbf{u}}_1) \quad \text{and} \quad \dot{\mathbf{w}}_3 = \phi(\dot{\mathbf{u}}_2 - \dot{\mathbf{u}}_3),$$

which describe the flow of water with respect to sand and clay, respectively. Likewise,

$$\dot{\mathbf{q}} = \phi_c(\dot{\mathbf{u}}_3 - \dot{\mathbf{u}}_1) \quad \text{and} \quad \dot{\mathbf{r}} = \phi_s(\dot{\mathbf{u}}_1 - \dot{\mathbf{u}}_3)$$

denote the macroscopic velocities characterizing the movement of clay relative to the sand grains and vice versa, respectively. Since the relative flows are assumed to be of laminar type, the microscopic velocities can be expressed as

$$\mathbf{v}_1 = \boldsymbol{\alpha}_1 \dot{\mathbf{w}}_1 \quad \text{and} \quad \mathbf{v}_3 = \boldsymbol{\alpha}_3 \dot{\mathbf{w}}_3$$

and

$$\mathbf{s} = \boldsymbol{\beta}_1 \dot{\mathbf{q}} \quad \text{and} \quad \mathbf{t} = \boldsymbol{\beta}_3 \dot{\mathbf{r}},$$

where $\boldsymbol{\alpha}_1$ and $\boldsymbol{\alpha}_3$ are the fluid/sand and fluid/clay matrix coefficients, and $\boldsymbol{\beta}_1$ and $\boldsymbol{\beta}_3$ are the clay/sand and sand/clay matrix coefficients, respectively.

The total kinetic energy is given by the expression,

$$E_K = \frac{1}{2}\rho_f \iiint_{\Omega_f} \| \dot{\mathbf{u}}_1 + \mathbf{v}_1 \|^2 \, d\Omega + \frac{1}{2}\rho_f \iiint_{\Omega_f} \| \dot{\mathbf{u}}_3 + \mathbf{v}_3 \|^2 \, d\Omega +$$

$$\frac{1}{2}\rho_c \iiint_{\Omega_c} \| \dot{\mathbf{u}}_1 + \mathbf{s} \|^2 \, d\Omega + \frac{1}{2}\rho_s \iiint_{\Omega_s} \| \dot{\mathbf{u}}_3 + \mathbf{t} \|^2 \, d\Omega - \frac{1}{2}\rho_f \phi \| \dot{\mathbf{u}}_2 \|^2,$$

where Ω_f, Ω_c and Ω_s are the volumes of fluid, clay and sand grains, respectively. The term $(1/2)\rho_f\phi \| \dot{\mathbf{u}}_2 \|^2$ is subtracted since the contribution of the fluid must be considered only once in the kinetic energy.

Following Leclaire *et al.* (1994), we define

$$m_{ij}^{(l)} \equiv \rho_f \iiint_{\Omega^{(l)}} \sum_k \alpha_{ki}^{(l)} \alpha_{kj}^{(l)} \, d\Omega, \qquad l=1,3,$$

where $\Omega^{(1)} = \Omega_c$, $\Omega^{(3)} = \Omega_s$, and

$$n_{ij}^{(1)} \equiv \rho_c \iiint_{\Omega_c} \sum_k \beta_{ki}^{(1)} \beta_{kj}^{(1)} \, d\Omega, \qquad n_{ij}^{(3)} \equiv \rho_s \iiint_{\Omega_s} \sum_k \beta_{ki}^{(3)} \beta_{kj}^{(3)} \, d\Omega.$$

Assuming statistical isotropy, we obtain $m_{ij}^{(l)} = m_l\delta_{ij}$ and $n_{ij}^{(l)} = n_l\delta_{ij}$; therefore (B3) simplifies to

$$E_K = \frac{1}{2}\rho_2 \| \dot{\mathbf{u}}_1 \|^2 + \rho_f\dot{\mathbf{u}}_1\cdot\dot{\mathbf{w}}_1 1 + \frac{1}{2}m_1 \| \dot{\mathbf{w}}_1 \|^2 + \frac{1}{2}\rho_2 \| \dot{\mathbf{u}}_3 \|^2 + \rho_f\dot{\mathbf{u}}_3\cdot\dot{\mathbf{w}}_3$$

$$+ \frac{1}{2}m_3 \| \dot{\mathbf{w}}_3 \|^2 + \frac{1}{2}\rho_3 \| \dot{\mathbf{u}}_1 \|^2 + \rho_c\dot{\mathbf{u}}_1\cdot\dot{\mathbf{q}} + \frac{1}{2}n_1 \| \dot{\mathbf{q}} \|^2 + \frac{1}{2}\rho_1 \| \dot{\mathbf{u}}_3 \|^2$$

$$+ \rho_s\dot{\mathbf{u}}_3\cdot\dot{\mathbf{r}} + \frac{1}{2}n_3 \| \dot{\mathbf{r}} \|^2 - \frac{1}{2}\rho_2 \| \dot{\mathbf{u}}_2 \|^2, \qquad (B4)$$

where

$$\rho_1 = \rho_s\phi_s, \qquad \rho_2 = \rho_f\phi, \qquad \rho_3 = \rho_c\phi_c.$$

Finally, expressing the kinetic energy as a function of $\dot{\mathbf{u}}_1$, $\dot{\mathbf{u}}_2$ and $\dot{\mathbf{u}}_3$, we get

$$
\begin{aligned}
E_K = \;&\frac{1}{2}(n_3\phi_s^2 - \rho_2 + m_1\phi^2 - \rho_3 + n_1\phi_c^2)\parallel\dot{\mathbf{u}}_1\parallel^2 \\
&+\frac{1}{2}(m_1\phi^2 + m_3\phi^2 - \rho_2)\parallel\dot{\mathbf{u}}_2\parallel^2 \\
&+\frac{1}{2}(n_1\phi_c^2 - \rho_2 + m_3\phi^2 - \rho_1 + n_3\phi_s^2)\parallel\dot{\mathbf{u}}_3\parallel^2 \\
&+(\rho_2 - m_1\phi^2)\dot{\mathbf{u}}_1\cdot\dot{\mathbf{u}}_2 + (\rho_2 - m_3\phi^2)\dot{\mathbf{u}}_2\cdot\dot{\mathbf{u}}_3 \\
&+(\rho_1 - n_3\phi_s^2 + \rho_3 - n_1\phi_c^2)\dot{\mathbf{u}}_1\cdot\dot{\mathbf{u}}_3. \qquad\text{(B5)}
\end{aligned}
$$

The generalized mass densities ρ_{ij} are obtained from the identification of the coefficients of expression (B5) with those of (B2). This gives

$$
\rho_{11} = \rho_s\phi_s a_{13} + (a_{21} - 1)\rho_f\phi + (a_{31} - 1)\rho_c\phi_c,
$$

$$
\rho_{22} = (a_{21} + a_{23} - 1)\rho_f\phi,
$$

$$
\rho_{33} = \rho_c\phi_c a_{31} + (a_{23} - 1)\rho_f\phi + (a_{13} - 1)\rho_s\phi_s, \qquad\text{(B6)}
$$

$$
\rho_{12} = -(a_{21} - 1)\rho_f\phi,
$$

$$
\rho_{23} = -(a_{23} - 1)\rho_f\phi,
$$

$$
\rho_{13} = -(a_{13} - 1)\rho_s\phi_s - (a_{31} - 1)\rho_c\phi_c,
$$

where

$$
a_{21} = \frac{m_1\phi}{\rho_f}, \qquad a_{23} = \frac{m_3\phi}{\rho_f}
$$

and

$$
a_{13} = \frac{n_3\phi_s}{\rho_s}, \qquad a_{31} = \frac{n_1\phi_c}{\rho_c}
$$

are the tortuosity parameters.

When there is no relative motion between the three phases, the following relationship holds

$$
\rho \equiv \rho_{11} + \rho_{22} + \rho_{33} + 2(\rho_{12} + \rho_{23} + \rho_{13}) = \rho_1 + \rho_2 + \rho_3,
$$

whence ρ may be viewed as the effective mass density.

Following Berryman (1980), we express the tortuosity parameters as

$$
a_{21} = \frac{\phi_s}{\phi}r_{12} + 1, \qquad a_{23} = \frac{\phi_c}{\phi}r_{23} + 1, \qquad a_{13} = \frac{\phi_c}{\phi_s}r_{13} + 1, \qquad a_{31} = \frac{\phi_s}{\phi_c}r_{31} + 1,
$$

where $r_{\nu\nu'}$ characterize the geometrical features of the pores ($r_{\nu\nu} = 1/2$ for spheres). Observe that, for instance, $a_{21} \to 1$ for $\phi \to 1$ and that $a_{21} \to \infty$ for $\phi \to 0$, as expected (Berryman 1980).

B.3 Friction coefficients

In order to obtain the viscous flow resistance coefficients b_{11} and b_{33}, we first consider the idealized situation when the solid part can be modelled as a dilute concentration of sand and clay spherical particles in the fluid. This situation is realized in the high-porosity limit ($\phi \to 1$). Since the concentration is dilute, each particle can be considered independently from the others. The viscous resistance force for a single sphere of radius R moving in a flow of average velocity v and a fluid viscosity η_f obeys Stokes's law,

$$F = 6\pi\eta_f vR.$$

Suppose that in a unit volume we have n_ν particles of radius R_ν, where $\nu = 1$ (sand grains) or 3 (clay particles). Then, the viscous resistance to the flow by particles of type ν can be written as

$$F_\nu = 6\pi\eta_f v n_\nu R_\nu. \tag{B7}$$

The density numbers n_ν can be thought of as the total volume of the particles of type ν divided by the volume of a single particle,

$$n_\nu = \frac{\phi_\nu}{\frac{4}{3}\pi R_\nu^3}. \tag{B8}$$

Substitution of (B8) into (B7) yields

$$F_\nu = \frac{9}{2}\eta_f v \phi_\nu R_\nu^{-2},$$

or, for the viscous resistance coefficient,

$$b_{\nu\nu} = F_\nu \frac{\phi^2}{v} = \frac{9}{2}\eta_f \phi^2 \phi_\nu R_\nu^{-2}. \tag{B9}$$

Note that the quantity

$$\kappa_\nu = \frac{2}{9}\frac{R_\nu^2}{\phi_\nu}$$

can be thought of as a partial permeability of the matrix formed by particles of type ν. Hence

$$b_{\nu\nu} = \eta_f \phi^2 \kappa_\nu^{-1}.$$

Equation (B9) provides an explicit expression for the resistance coefficients b_{11} and b_{33} in the high-porosity limit. At lower porosities it is customary to divide the expression for permeability by an empirical factor $10(1 - \phi)/\phi^3$, which yields permeability values consistent with the Kozeny–Carman empirical relationship (Berryman 1995). Then, κ_s and κ_c are equal to κ_1 and κ_3 divided by that factor. We thus write

$$b_{\nu\nu} = 45\eta_f R_\nu^{-2} \phi^{-1}(1 - \phi)\phi_\nu$$

or

$$b_{11} = 45\eta_f R_s^{-2} \phi^{-1}(1 - \phi)^2(1 - C),$$

$$b_{33} = 45\eta_f R_c^{-2} \phi^{-1}(1 - \phi)^2 C,$$

where R_s and R_c denote the average radii of sand and clay particles, respectively.

References

Batzle M. and Wang Z. 1992. Seismic properties of pore fluids. *Geophysics* **57**, 1396–1408.

Berryman J.G. 1980. Confirmation of Biot's theory. *Applied Physical Letters* **37**, 382–384.

Berryman J.G. 1995. Mixture theories for rock properties. In: *Rock Physics and Phase Relations: A Handbook of Physical Constants*, pp. 205–228. American Geophysical Union.

Biot M.A. 1962. Mechanics of deformation and acoustic propagation in porous media. *Journal of Applied Physics* **33**, 1482–1498.

Brown R.J.S. and Korringa J. 1975. On the dependence of the elastic properties of a porous rock on the compressibility of a pore fluid. *Geophysics* **40**, 608–616.

Carcione J.M. and Seriani G. 1998. Seismic velocities in permafrost. *Geophysical Prospecting* **46**, 441–454.

Dutta N.C. and Ode H. 1983. Seismic reflections from a gas–water contact. *Geophysics* **48**, 148–162.

Dvorkin J., Nolen-Hoeksema R. and Nur A. 1994. The squirt-flow mechanism: macroscopic description. *Geophysics* **59**, 428–438.

Fedorov F.I. 1968. Theory of Elastic Waves in Crystals. Plenum Press.

Goldberg I. and Gurevich B. 1998. A semi-empirical velocity-porosity-clay model for petrophysical interpretation of P- and S-velocities. *Geophysical Prospecting* **46**, 271–285.

Han D.H., Nur A. and Morgan D. 1986. Effects of porosity and clay content on wave velocities in sandstones. *Geophysics* **51**, 2093–2107.

Klimentos T. and McCann C. 1990. Relationships among compressional wave attenuation, porosity, clay content, and permeability in sandstones. *Geophysics* **55**, 998–1014.

Krief M., Garat J., Stellingwerff J. and Ventre J. 1990. A petrophysical interpretation using the velocities of P and S waves (full waveform sonic). *The Log Analyst* **31**, 355–369.

Leclaire Ph., Cohen-Ténoudji F. and Aguirre-Puente J. 1994. Extension of Biot's theory of wave propagation to frozen porous media. *Journal of the Acoustical Society of America* **96**, 3753–3768.

Tosaya C. and Nur A. 1982. Effects of diagenesis and clays on compressional velocities in rocks. *Geophysical Research Letters* **9**, 5–8.

Xu S. and White R. 1995. A new velocity model for clay–sand mixtures. *Geophysical Prospecting* **43**, 91–118.

Zimmerman R.W., Somerton W.H. and King M.S. 1986. Compressibility of porous rocks. *Journal of Geophysical Research* **91**, 765–777.